



**Environmental  
Science**  
Nano

**Effects of pH and Electrolytes on the Sheet-to-Sheet  
Aggregation Mode of Graphene Oxide in Aqueous Solutions**

Journal:	<i>Environmental Science: Nano</i>
Manuscript ID	EN-ART-11-2019-001365.R2
Article Type:	Paper

SCHOLARONE™  
Manuscripts

**Environmental significance statement**

The extensive use of graphene oxide (GO) will inevitably lead to its release into the water environment. Thus, a detailed understanding of the aggregation behavior under different aqueous environment is critical for predicting the toxicity. Also, revealing the aggregation pattern is valuable for elucidating the aggregation mechanisms of GO-based materials and providing theoretical foundations for its application in wastewater treatment. Furthermore, the combination of molecular dynamics simulations and density functional theory calculations in this study provides a platform for the application of theoretical methods in other aqueous environmental issues.



## Effects of pH and Electrolytes on the Sheet-to-Sheet Aggregation Mode of Graphene Oxide in Aqueous Solutions

Huan Tang<sup>a,b\*</sup>, Shuyan Zhang<sup>a,b</sup>, Tinglin Huang<sup>a,b\*</sup>, Fuyi Cui<sup>c</sup>, and Baoshan Xing<sup>d</sup>

Received 00th January 20xx,  
Accepted 00th January 20xx

DOI: 10.1039/x0xx00000x

[www.rsc.org/](http://www.rsc.org/)

In this work, the aggregation mode of graphene oxide (GO) was identified. Atomic force microscope (AFM) characterizations indicated that protonation under lower pH was more efficient in accelerating the stacking of GO than binding with metal ions, and molecular dynamics (MD) simulations revealed this should be attributed to the different favorable aggregation mode under different aqueous chemistries. GO tended to aggregate in the face-to-face or partial face-to-face mode at lower pH, and partial face-to-face, edge-to-edge, or point-to-point mode at higher pH with the presence of metal ions. To elucidate the mechanisms that pH and metal ions can exert distinct effect on the aggregation mode of GO, density functional theory calculations were performed. The results demonstrated that the favorable face-to-face and partial face-to-face aggregation at lower pH was mainly guided by the stronger  $\pi$ - $\pi$  interaction and suppressed water-mediated steric hindrance, however, hydrogen bond and vdWs interactions were not important in determining the aggregation mode. Overall, the distinct aggregation mode of GO under different aqueous chemistries will shed light on predicting the toxicity and environmental applications of GO.

### Introduction

Graphene oxide (GO), featuring a thin (0.3 to 1.4 nm) two-dimensional structure and contains many oxygen containing functional groups (including epoxide, hydroxyl, carbonyl, and carboxyl groups)<sup>1, 2</sup>, has been used for a variety of applications owing to its unique electronic, thermal, and mechanical properties<sup>3-5</sup>. Moreover, GO-based materials are receiving increasing attention for environmental use in the fields of membrane filtration<sup>6</sup>, photocatalytic<sup>7</sup>, and adsorption<sup>8</sup>. Consequently, the production growth of this material is very rapid<sup>9</sup>, and GOs are expected to eventually reach sensitive aquatic environment<sup>10, 11</sup>. The toxicity of GO towards organisms has been reported by various studies and was found to related to its aggregation<sup>12-14</sup>. Thus, investigation on GO aggregation is of great importance to predict its adverse effects. Additionally, GO has shown great potential in wastewater treatment, such as membrane filtration and organic pollutant removal<sup>15-19</sup>. Given that there is a strong correlation between GO architecture and its mechanical, chemical, and sorptive properties,<sup>20, 21</sup> a deep

understanding of GO aggregation will contribute to its environmental applications.

Recently, tremendous efforts have done to understand the aggregation of GO in aqueous media<sup>10, 22, 23</sup>. Dynamic light scattering was commonly used to explore the aggregation kinetics, and the ranges of critical coagulation concentrations (CCC) reported for GO in aqueous media were 38 to 200 mmol/L of NaCl and 0.9 to 2.6 mmol/L of CaCl<sub>2</sub><sup>24, 25</sup>. Based on these CCC values, GO will aggregate in some surface waters and groundwater<sup>11, 26</sup>. Yang et al. investigated the morphological transformation of GO under heavy metal ions and reported that the aggregation of the GO was not only an accumulative process via electric double-layer suppression but also accompanied by structural transformation of GO into 1D, 2D, and 3D nanomaterials<sup>24</sup>. However, the detailed sheet-to-sheet interaction mode was still unknown. Aqueous chemistry was reported to play key roles in determining the aggregation kinetic of GO, but limited efforts have been devoted to correlate the aqueous chemistry with the sheet-to-sheet aggregation mode. Two fundamental aggregation geometries of interacting GO sheets have been proposed (edge-to-edge and face-to-face)<sup>21, 27</sup>, and the favourable aggregation mode was speculated to be mediated by aqueous chemistries. Understanding the aggregation mode in different aqueous chemistries and associate it with its corresponding properties is critical to predict GO behaviour. Thickness, which is related to the aggregation of GO, is an important factor in determining the toxicity: in the studies on bacterium *E. coli*<sup>28</sup> and human endothelial cells<sup>29</sup>, the strong cytotoxicity of GO was reported to be related to its great dispersibility and smaller aggregate size, all of which increases direct contact with cells and induces greater intracellular oxidative stress<sup>30</sup>; in the studies on algae growth, the significant shading effect was also due to that GO was dispersed

<sup>a</sup> Address here Key Laboratory of Northwest Water Resource, Environment and Ecology, MOE, Xi'an University of Architecture and Technology, Xi'an, 710055, China.

<sup>b</sup> Shaanxi Key Laboratory of Environmental Engineering, Xi'an University of Architecture and Technology, Xi'an, 710055, China.

<sup>c</sup> College of Urban Construction and Environmental Engineering, Chongqing University, Chongqing, 40045, China.

<sup>d</sup> Stockbridge School of Agriculture, University of Massachusetts, Amherst, MA, 01003, USA

\* E-mail: tanghuan@xauat.edu.cn, Tel/ Fax: +86-29-82207886 (Huan Tang).

E-mail: huangtinglin@xauat.edu.cn, Tel/ Fax: +86-29-82201038 (Tinglin Huang).

Electronic Supplementary Information (ESI) available: [Additional information regarding synthesis of GO, AFM images, DFT results, and MD results are included]. See DOI: 10.1039/x0xx00000x

in water as individual GO sheets<sup>12, 14</sup>. Under certain chemical conditions in water, aggregation of GO may happen. Thus, the toxicity of GO may be changed upon aggregation and is speculated to be related to the aggregation mode. If GOs aggregate in face-to-face mode, the shading area will be decreased, and the aggregation will weaken GO toxicity; however, if GO aggregate in edge-to-edge mode, then the shading effect will not be alleviated significantly, and the aggregation will not affect GO toxicity. Except for predicting the toxicity, elucidating the GO aggregation morphology will provide theoretical basis for its environmental applications<sup>31</sup>. To develop effective adsorption technologies, there must be a better understanding of the linkage among aggregation and adsorption properties. Previous studies showed in the adsorption of aromatics on single-layered GO, wrinkles, holes, and edges are favourable adsorption sites<sup>32</sup>. Upon aggregation, some of these sites may be covered and new type of adsorption sites will be formed. Face-to-face aggregation will reduce the number of accessible wrinkles and holes and create micropores and mesopores which are also important sorption sites for organic contaminants, thus the adsorption mechanism and adsorption capacity maybe changed. However, edge-to-edge aggregation will exert negligible effect on the accessible binding sites. In summary, it is of both scientific curiosity and technical importance to know how GO sheets aggregate in different aqueous chemistries and correlate the aggregation morphology with its relevant properties.

To explore the aggregation mode, characterization methods such as atomic force microscopy (AFM) that allows microscopic details to be characterized should be employed, and complementary information to experimental studies is also needed. Recently, molecular dynamic (MD) simulations and density functional theory (DFT) calculations have been combined with experimental characterizations to provide details at molecular level<sup>23, 32-37</sup>. For example, in exploring how the graphene nanosheets penetrate and extract phospholipids from the cell membranes, transmission electron microscopy was used to explore the rough destructive extraction stages, and MD simulations to reveal the atomic details of the process.<sup>34</sup> The interactions between humic acid fractions and GO at the molecular level were elaborated combining AFM and DFT<sup>38</sup>. In our previous study, AFM characterization was employed to search for the most favourable adsorption sites of aromatic compounds on GO, and MD combined with DFT simulations were used to investigate the dynamic searching process and uncover the mechanisms.<sup>32</sup> Therefore, it is reasonable to explore the GO aggregate morphology combining experimental characterization, MD simulation, and DFT calculation.

Based on the above discussion, GO aggregate modes under different aqueous chemistries were explored systematically. AFM characterization was employed to give a rough view of the aggregate morphology, along with MD simulations used to provide microscopic morphology details and DFT calculations to uncover the mechanisms.

## Experimental

### Synthesis of Graphene Oxide

GO was synthesized through the reaction of graphite powder (Nanjing XFNANO Materials Tech Co., Ltd.) with  $\text{KMnO}_4$  in a concentrated  $\text{H}_2\text{SO}_4$  solution (the Hummers method).<sup>39</sup> Detailed preparing method is the same with our previous study<sup>37, 40</sup> and is shown in part 1 in Electronic Supplementary Information (SI 1).

### Aqueous Chemistry and AFM Characterizations

Previous studies concluded that the aggregation of GO is highly dependent on pH and ionic strength,<sup>4, 13</sup> therefore, aqueous pH and the presence of metal cations were considered in this study. According to that the significant aggregation of GO happened at  $\text{pH} < 4$ <sup>40</sup> and that the range of pH usually observed in aquatic environment is 5~9<sup>41</sup>, pH of 3, 6 and 9 were selected in the current study. Electrokinetic measurements showed GO remains negatively charged over the whole pH range,<sup>24, 40</sup> and deprotonation also happens at  $\text{pH} < \text{pKa}$ . Thus, a small quantity of carboxylic groups will be deprotonated at pH 3. At pH 6, most of the carboxylic groups will be deprotonated; at pH 9, all the carboxylic groups will be deprotonated. Solution pH of GO (20 mg/L) was adjusted by adding negligible volumes of 0.1 mol/L HCl or NaOH solution. The CCC values of the GO we use are 110 mM NaCl and 2.66 mM  $\text{CaCl}_2$ ,<sup>40</sup> therefore, 60 mM, 200 mM NaCl, 1.5 mM, or 5 mM  $\text{CaCl}_2$  were selected to generate slight and significant aggregations of GO. To study the combined effect of pH and metal cations, pH of GO solutions (40 mg/L) were first adjusted to 2.7, 5.7, or 9.0 and then were mixed with equal volumes of NaCl (120 mM or 400 mM) or  $\text{CaCl}_2$  (3 mM or 10 mM). After mixing, the pH values were ~3, 5.8, and 6.5 and were then adjusted to 3, 6, and 9. Electrophoretic mobilities (EPM) of GOs were measured with a Zeta Sizer Nano ZS (Malvern Instrument, Worcestershire, U.K.).

The morphology of GO aggregate was examined using a Bruker BioScope Atomic Force Microscope (AFM). Before characterizations the solutions were prepared and standing for 10 min, and then 3  $\mu\text{L}$  of the solution were dripped onto the mica plates and dried for 10 min for AFM measurements. Preliminary experiment and previous studies<sup>24</sup> showed long aggregation time will result in the formation of sphere-like tight GO aggregates and it was hard to distinguish the GO sheet, and 10 min is appropriate for exploring the sheet-to-sheet aggregation mode. It should be noted that the drying condition is ambient temperature and pressure, and ultra- high or low high temperature and pressure may have notable impacts on measurements. During the drying, samples were covered by a watch glass for protection from dust. To strengthen the AFM evidence, AFM measurements for each condition were carried out triplicate with samples prepared at different times, and images were taken at several random locations across the sample.

### MD Simulation

GOs used for MD simulations were built based on the Lerf-Klinowski model<sup>42</sup>: GO sheet is a network of benzene rings, bearing epoxy (-O), hydroxyl (-OH), and carboxylic (-COOH) groups. Epoxy and hydroxyl are the nearest neighbours and located at the opposite sides of the basal plane,<sup>43</sup> and carboxylic groups are at the periphery of the GO platelets. Basic model of GO was set to  $\text{C}_{20}(\text{-O})_2(\text{-OH})_2(\text{-COOH})_1$ , similar model has been employed by other

studies and was proved to perform well for exploring the properties of GO<sup>40, 44, 45</sup>.  $C_{20}(-O)_2(-OH)_2(-COO^-)_{0.1}(-COOH)_{0.9}$ ,  $C_{20}(-O)_2(-OH)_2(-COO^-)_{0.9}(-COOH)_{0.1}$ , and  $C_{20}(-O)_2(-OH)_2(-COO^-)_1$  were used to mimic the behaviour of GO at pH 3, 6 and 9, respectively (there may be discrepancy between the exact quantity of deprotonated carboxylic groups between our models and the real situation in water environment but will not affect the mechanism understanding). 5 mM Na<sup>+</sup> and Cl<sup>-</sup> were added to compensate for the net charges in the simulation box. Simulation boxes with the size of  $\sim 14.0 \times 14.0 \times$

14.0 nm<sup>3</sup> contain  $\sim 80000$  water molecules were built (Fig. 1a-b), and GOs with different sizes were used (Fig. 1c). The model of GO used in current study is flat and no wrinkles or imperfections were included. A system containing GO with wrinkles or imperfections will include a great many of water molecules and need ultra-long simulation times, which is difficult at present. To mimic the effect of metal ions on the aggregation of GO, 60 mM NaCl, 200 mM NaCl, 1 mM CaCl<sub>2</sub>, or 5 mM CaCl<sub>2</sub> was added to the box.

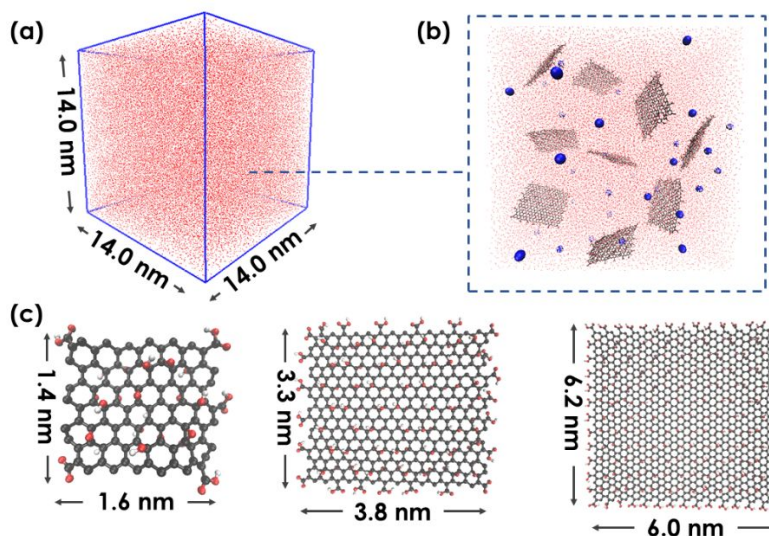


**Fig. 1.** Setup of the MD simulation system. (a) Dimension of the simulation system. (b) Initial setup for the aggregation of GO. (c) Models of GOs with different sizes. H in white, O in red, C in black, the tiny red dots represent water molecules, and the blue balls represent metal ions.

The optimized potentials for the liquid simulations—all atoms (OPLS-AA) force field<sup>46</sup> implemented in the GROMACS software package<sup>47</sup> was used for simulating the aggregation of GO. Water molecules were simulated using the standard SPC/E model.<sup>48</sup> Bond lengths were constrained with LINCS<sup>49</sup> and water geometries were constrained with SETTLE.<sup>50</sup> The cutoff for vdWs interaction was set to 1.0 nm. Short-range electrostatic interactions were directly calculated using the Coulomb law. Long-range electrostatic interactions beyond 1.0 nm were accounted for employing the particle-mesh Ewald method.<sup>51</sup> For each system, static structure optimization was first performed to ensure that the maximum force is less than 1,000 kJ/(mol·nm). Then the systems were equilibrated for 100 ps at a temperature of 300 K (NVT) followed by a constant pressure of 1 bar (NPT). During the minimization and equilibration processes, the basal planes of the GO sheets were constrained. Then, GOs were released and MD simulations were performed. In the course of production runs, the pressure was coupled to an isotropic Parrinello - Rahman barostat<sup>52</sup> and the temperature was regulated using the Nose - Hoover thermostat<sup>53</sup>. For equilibration purposes, a Berendsen thermostat<sup>54</sup> was implemented to keep the system at constant pressure. The equations of motion were integrated with a time step of 2 fs using the leap-frog algorithm<sup>42</sup> and data were collected every 100 ps. Periodic boundary conditions were applied in all three directions. The criteria for the formation of a hydrogen bond (H-bond): the donor-acceptor distance is smaller than 0.35 nm and the hydrogen-donor-acceptor angle is less than 30 degree.<sup>47, 55</sup> This criterion for H-bond has been used in previous studies.<sup>56-58</sup>

### DFT Calculation

DFT calculations were performed using Gaussian09 program.<sup>59</sup> Geometric optimizations were calculated using B3LYP functional with the 6-311+G\*\* basis set, and DFT-D3(BJ) dispersion correction and SMD implicit solvent model was employed. LOLIPOP (Localized Orbital Locator Integrated Pi Over Plane) index was calculated using Multiwfn<sup>60</sup> to measure the  $\pi$ -stacking abilities of GO. Isotropic average polarizability was employed to examine the vdWs intensity and was calculated on the level of PBE1PBE/aug-cc-pVTZ. Based on Gaussian output, Isotropic average polarizability was obtained using Multiwfn (function 7 of main function200). DFT calculations are time-consuming, and therefore, smaller GO models were used (SI2). Considering specific interactions that involve water cannot be described by implicit solvation, explicit water molecules were also included. During the aggregation, there will be two kinds of H-bond interaction between GOs: (1) H-bonds forming directly between the functional groups (GO $\cdots$ GO); (2) water-bridged H-bonds forming between GOs (GO $\cdots$ water $\cdots$ GO). Therefore, two sets of DFT calculation systems were built (Fig. S3) to explore the H-bond interaction. Additionally, the detailed edge-to-edge interaction was calculated using DFT. Relevant DFT system setups are provided in SI2.

### Results and discussion

## AFM Results of GO Aggregate Under Different Aqueous chemistries

At pH~3 where most of the carboxy groups are protonated, GOs thickness is 3~12 nm (Fig. 2a). Considering that the height of single layer GO was around 0.7 nm (Fig. S5a), the height of 3~12 nm corresponds to about 4 to 17 stacked GO sheets and a significant aggregation of GO. One may doubt that the stackings in AFM images were formed during imaging and are not related to the actual aggregation in water. To address this question, we can compare the AFM results at pH~3 with these of pH~6 and pH~9 (Fig. 2b-d).

At pH ~6 where most of the carboxy groups are deprotonated and no metal cations were added, no obvious stacking were witnessed in the AFM images (Fig. S5b). Previous stability studies concluded that GOs tend to keep stable in water at pH ~6<sup>26, 61</sup>, demonstrating the several aggregations of GOs in the AFM images are occurred during the drying process. It should also be noticed that the maximum thickness of the aggregates can only reach to ~1.5 nm, proving the thick stackings of GO observed at pH ~3 in the AFM images are mainly occurred in water before deposition on the substrate.

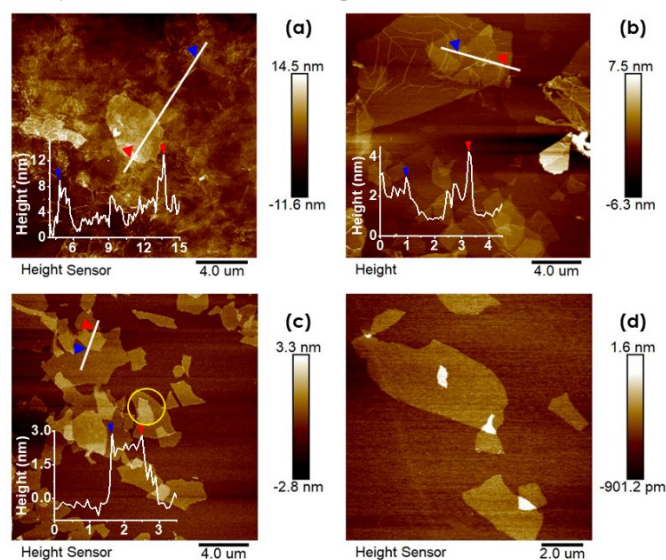


**Fig. 2.** AFM characterizations of the aggregation of GO under (a) pH~3, (b) pH~6 with 1 mM CaCl<sub>2</sub> and (c) pH~9 with 1 mM CaCl<sub>2</sub>. Heights measured between the red and blue arrows are presented on the AFM images. (d) Face-to-face and partial face-to-face aggregation of GOs with contrasting sizes at pH~6 with 1 mM CaCl<sub>2</sub>.

When we add 60 mM NaCl or 1 mM CaCl<sub>2</sub> at pH ~6, aggregates with the thickness of 2~4 nm were observed (Fig. 2b and Fig. S5c).

At pH ~9 where all the carboxy groups are deprotonated and 60 mM NaCl or 1 mM CaCl<sub>2</sub> were added, thickness of GO aggregates was 2~3 nm (Fig. 2c and Fig. S5d).

The above AFM results indicate stackings of GOs under lower pH regimes are thicker than these under high ionic strength, implying protonation is more efficient than binding with metal ions in accelerating the stacking of GO. Here raises a question that if the distinct aggregate thickness is caused by the electrostatic repulsions between GOs, for specifically, if the GO solution at pH ~3 is less negative than that at pH 6 with 60 mM NaCl or 1 mM CaCl<sub>2</sub>? Electrokinetic measurements showed the EPMS of GO at pH 3, pH 6

with 60 mM NaCl, and pH 6 with 1 mM CaCl<sub>2</sub> was  $(-2.47 \pm 0.13) \times 10^{-8}$ ,  $(-2.39 \pm 0.05) \times 10^{-8}$ , and  $(-1.94 \pm 0.09) \times 10^{-8} \text{ m}^2 \text{ V}^{-1} \text{ s}^{-1}$ , respectively. This result demonstrated that the more significant stacking under lower pH is not determined by the electrostatic repulsions between GOs.

To explore the mechanisms of the distinct effect of pH and metal ions, theoretical calculations were employed. First, MD simulations were performed to evidence AFM results and provide details for the aggregate morphology.

## MD Results of the Combined Effect of pH and Metal Cations on Aggregation Mode

As shown in Fig. 3, four kinds of aggregate mode during the aggregation process were revealed by MD simulations: face-to-face, partial face-to-face, edge-to-edge, and point-to-point.

At pH ~3, GOs aggregated quickly and formed multi-layered aggregate (Fig. S6a), with face-to-face and partial face-to-face as the dominant aggregate mode. For the face-to-face mode (Fig. 3a), two GO planes paralleled to each other and the interlayer distance between the two GO single layers is ~0.7 nm, according well with previous studies<sup>45</sup>. There is a layer of water molecules confined within the interlayer maintained by H-bonds and form a sandwich-like GO-water-GO structure. This face-to-face aggregate morphology helped to maximize the vdWs, H-bond, and  $\pi$ - $\pi$  interaction between GO layers. For the partial face-to-face mode, angles less than 90° were observed between the two GO planes (Fig. 3b and Fig. S8a, b, d), interlayer distance was larger than that of face-to-face mode (0.7 nm), and plenty of water molecules were confined between the two layers forming water-bridged H-bonds networks (blue dashed lines in the Figure) with GO.

Dynamic aggregation process indicated that the face-to-face morphology was accomplished via a “bind and adjust” two-step mechanism in which two GOs firstly bind with each other and subsequently adjust to maximize the interacting area. For instance (Fig. S7), two GOs aggregated in partial face-to-face mode in the early aggregation process; then the two GOs diffused and repelled the water molecules, adjusting to the face-to-face mode and maximizing the interacting area. This face-to-face mode helped to increase the thickness of GO aggregate, corresponding to the thick stackings observed in AFM characterizations at pH ~3. Here raises a question that whether all the non-face-to-face mode can adjust to the face-to-face mode if the simulation time is sufficient? To address this issue, we extended the simulation to another 50 ns upon the aggregation of GOs and the results indicated that the aggregate morphology was predominantly relate to the aqueous chemistries and GO property, as will be elaborated in the following discussions.

At pH ~6 and no metal cations were added, the negatively charged GO kept stable and no aggregation were observed (Fig. S6b), consistent with previous stability studies<sup>26, 61, 62</sup>. The thickness of ~1.5 nm in Fig. S5b corresponding to the stacking of 2 layers of GO. According to the above MD results that no aggregation happened at pH 6 without the presence of metal ions, it is concluded that the stacking observed in the AFM image mainly occurred during imaging.

When we add 60 mM NaCl or 1 mM CaCl<sub>2</sub> at pH ~6, GOs tended to stack in the partial face-to-face mode (Fig. S6c and Fig. S8a, d)

and face-to-face morphology only occurred for GOs with contrasting sizes (Fig. S8c), correlating well with the AFM results (Fig. 2b, d and Fig. S5c). To examine whether face-to-face aggregation can occur at pH  $\sim$ 6 at ultra-high ion strength and sufficient simulation time, we increased the concentration of NaCl and CaCl<sub>2</sub> to 200 mM and 5 mM and extend the simulation time to another 50 ns. However, surprisingly, GOs with the same size still stacked together in the partial face-to-face mode (Fig. S8b) (AFM evidence was provided in Fig. S5f-g). This interesting phenomenon can be elucidated by the aggregation mechanism. Aggregation of GOs was initiated at a binding point and then the GOs diffuse to maximize the overlapping area. Several kinds of binding points were observed, for example, oxygen-containing functional groups that can facilitate H-bond or water-bridged H-bond interactions, benzene rings that can facilitate  $\pi$ - $\pi$  interactions, or any pair of atoms that can facilitate

vdWs interactions. Also, it should be mentioned that the initial binding points were mainly near the protonated carboxyl groups. During the diffusion, the strong electrostatic repulsion near edges will resist stacking or overlapping between layers. Additionally, the abundant water molecules will form H-bond network with functional groups on GO, screening the attractive forces and restraining the face-to-face aggregation. For GOs with contrasting sizes, once the binding point was located on the basal plane of GO, the electrostatic repulsion between the edges of the two sheets would lock them into completely overlapped. Thus, face-to-face aggregation is more accessible for GO with contrasting sizes. Metal ions played two roles during the aggregation: firstly, neutralizing the negative charges and screening the long-range electrostatic repulsion; secondly, Ca<sup>2+</sup> helped to bridge GOs by interacting with the oxygen-containing functional groups (Fig. S9 a,b).

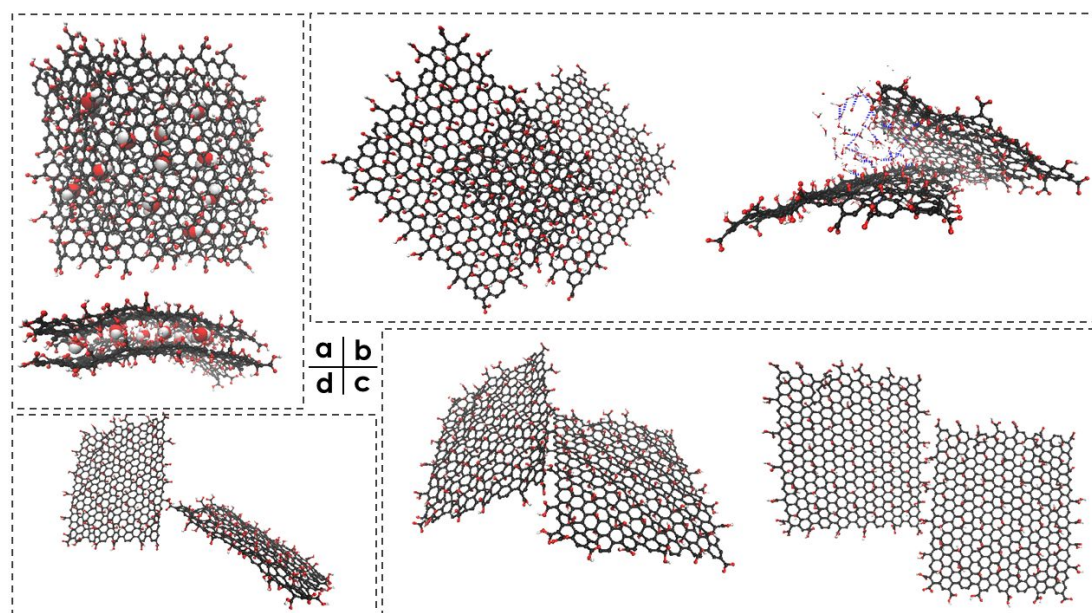


**Fig. 3.** MD results of the aggregate mode. (a) Top view and side view of the face-to-face aggregation. Water molecules are highlighted using spherical models, and not all the water molecules are shown to increase clarity. (b) Top view and side view of the partial face-to-face aggregation. Blue arrows indicate H-bonds. (c) Two modes of edge-to-edge aggregation. (d) Point-to-point aggregation.

At pH  $\sim$ 9 and 60 mM NaCl or 1 mM CaCl<sub>2</sub> were added, MD results indicated that edge-to-edge and point-to-point aggregation dominated, and only a few partial face-to-face aggregations occurred (Fig. 3c, Fig. S6d and Fig. S8e, f). For the edge-to-edge mode, GOs were connected through a “line” of interaction and two forms were witnessed (Fig. 3c and Fig S9): (I) there was an angle between the two GO planes and the “line” was maintained by chelating interaction between metal ions and carboxyl groups (Fig. S9c-d); (II) two GO planes were almost in the same plane and the “line” was maintained by direct H-bond or water-bridged H-bonds between carboxyl groups located at the edges (Fig. S9e-f). For the point-to-point mode (Fig. 2d), two GOs interacted at a point through H-bond, vdWs, or  $\pi$ - $\pi$  interaction. The point-to-point aggregation was not stable, and single GO particle tended to hop back into bulk solution upon aggregation, executes a rapid three-dimensional random walk, re-encounters the GO where it may reaggregate, potentially

repeating this process multiple times and no stable aggregate formed (Fig. S10). Additional to the edges, the point-to-point aggregation was also observed on the basal plane (Fig. S8g). This kind of point-to-point aggregation seems like face-to-face aggregation in the looking-down perspective, which may help to explain the “face-to-face” aggregation (yellow circled) in Fig. 2(c).

Combining the above AFM and MD results, it was reasonable to conclude that protonation is more effective than binding with metal ions in accelerating the stacking of GO. More specifically, at pH  $\sim$ 3 with most functional groups are protonated, GOs tended to aggregate in the face-to-face mode or partial face-to-face mode; however, at higher pH where most of the carboxyl groups are deprotonated, GOs tended to aggregate in other modes independent of the ionic strength and ion species. Experimental studies have established that Ca<sup>2+</sup> was more efficient than Na<sup>+</sup> in accelerating the aggregation kinetic of GOs, however, the MD simulation results indicated Ca<sup>2+</sup> and Na<sup>+</sup> showed no significant difference in mediating the aggregation mode.

To be specific, both  $\text{Ca}^{2+}$  and  $\text{Na}^{+}$  failed to facilitate the face-to-face aggregation of GO. One may doubt that  $\text{Ca}^{2+}$  can bridging the GOs through alkoxide or dative bonds with hydroxyl groups and accelerate the face-to-face aggregation. However, the binding between  $\text{Ca}^{2+}$  and hydroxyl was weak and unstable compared to the binding between  $\text{Ca}^{2+}$  and carboxyl, especially with the interference of water molecules in the interlayers. To make it more convictive, we calculate the binding energy of  $\text{Ca}^{2+}$  with carboxyl and hydroxyl. The binding energy was -57.80 kcal and -303.81kcal for  $\text{Ca}^{2+}$ -hydroxyl and  $\text{Ca}^{2+}$ -carboxyl, respectively. This significance on interaction energy indicated that it was more favourable for  $\text{Ca}^{2+}$  to interact with carboxyl located at the edges of GO. Therefore, it would be favourable for  $\text{Ca}^{2+}$  to bridging the edges of GO than bridging the basal plane.

Given that the aggregation was governed by the interactions involved during the aggregation process (e.g.,  $\pi$ - $\pi$ , H-bond, vdWs), it was speculated that pH and metal ions can exert distinct effect on these interactions. To verify this speculation, we performed DFT calculations to examine how pH and metal ions affect these forces.

### Effect of pH and Metal Cations on the Interactions Involved during Aggregation

#### $\pi$ - $\pi$ interaction

$\pi$ - $\pi$  interaction governs a variety of structural phenomena such as self-assembly process and crystal packing of organic molecules.<sup>63</sup> Therefore, it was speculated that pH and metal cations can exert

distinct effects on the  $\pi$ - $\pi$  interaction ability of GOs. Jérôme et al. proposed an index, named as LOLIPOP (Localized Orbital Locator Integrated Pi Over Plane), to measure the  $\pi$ -stacking ability of aromatic systems, and showed that a ring with smaller LOLIPOP value has stronger  $\pi$ - $\pi$  interaction ability.<sup>64</sup> LOLIPOP values of each benzene ring in GO were calculated using Multiwfn<sup>60</sup> to explore the effect of protonation and metal cations on the  $\pi$ - $\pi$  interaction strength of GO.

Four systems were built: GO with four carboxyl groups deprotonated (I), GO with four carboxyl groups protonated (II), GO with four carboxyl groups deprotonated and the presence of  $\text{Ca}^{2+}$  (III), and GO with four carboxyl groups deprotonated and the presence of  $\text{Na}^{+}$  (IV) (The choice of number of ions is to neutralize the negative charges of GO. Preliminary calculations were performed to examine the effect of number and position of metal ions on the calculation results, and no significant effect was observed). LOLIPOP values of benzene rings in different systems were provided in Fig. 4. Compared to the deprotonated GO, LOLIPOP values of the benzene rings decreased upon protonation, indicating that the  $\pi$ - $\pi$  interaction ability of the benzene rings are increased at lower pH. However, this trend was not significant when  $\text{Ca}^{2+}$  or  $\text{Na}^{+}$  was added; and for benzene 3, 5, 6, and 8, the  $\pi$ - $\pi$  interaction ability was even impaired. Therefore, it was concluded that protonation is more efficient in accelerating the  $\pi$ - $\pi$  interaction and  $\pi$ - $\pi$  interaction is an essential factor that induce the distinct effect of protonation and metal cations.

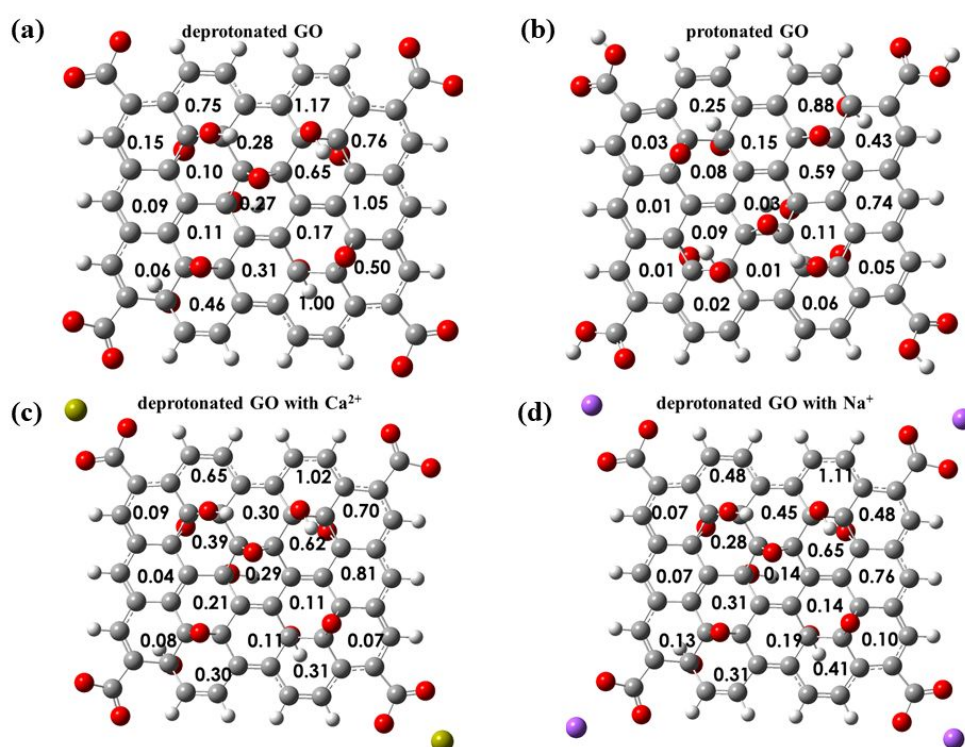


**Fig. 4** LOLIPOP values of the benzene rings in GO. (a) GO with carboxyl groups deprotonated. (b) GO with carboxyl groups protonated. (c) GO with carboxyl groups deprotonated and the presence of  $\text{Ca}^{2+}$ . (d) GO with carboxyl groups deprotonated and the presence of  $\text{Na}^{+}$ .

In previous studies, the accelerated aggregation of GO at low pH was always attributed to the reduction in the electrostatic repulsive

forces between GO as predicted by colloidal theory,<sup>26</sup> the above results implied that the increased  $\pi$ - $\pi$  interaction between GO is also

an important mechanism. Additionally, it should be noted that the coordination with metal ions not only screen the negative charges GO carries, but also affect the  $\pi$ - $\pi$  interaction intensity between GOs. Therefore, the effect of metal ions and pH on  $\pi$ - $\pi$  interaction should be considered in future studies concerning materials that contain benzene rings.

#### van der Waals

vdWs force, which is caused by the inhomogeneous distribution of electron density in molecules, also serves as a driving force during the aggregation process. Though vdWs interaction is weak, its long-range nature and collective effect can be important in the aggregation of GO. To investigate how the protonation and binding with metal ions exert effect on the vdWs intensity, isotropic average polarizabilities of GOs are calculated. GO is polar and the vdWs between GOs is mainly determined by dispersion interaction. Dispersion interaction is related to the isotropic average

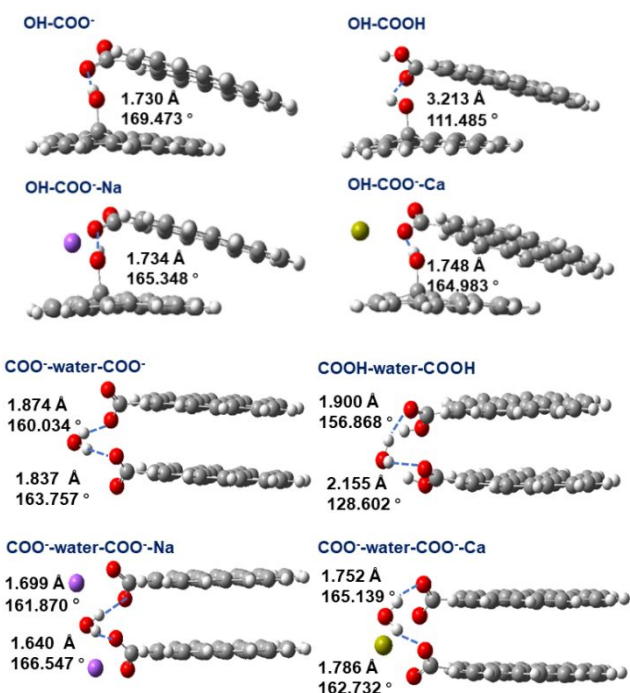


**Fig. 5.** Effect of protonation and metal ions on the intensities of direct and water-bridged H-bonds. Blue dashed lines indicate H-bonds. OH-COO<sup>-</sup> means the direct H-bond interaction between hydroxy and deprotonated carboxyl. OH-COO<sup>-</sup>-Na means the direct H-bond interaction between hydroxy and deprotonated carboxyl with the presence of Na<sup>+</sup>. polarizability<sup>65</sup>, and therefore, the value of isotropic average polarizability can be used to evaluate the vdWs of GO.

As shown in Table S1, the polarizability of GO increased upon protonation, implying that the vdWs interaction between GOs will be accelerated at low pH. However, binding with Ca<sup>2+</sup> accelerated the vdWs intensity more significantly. Notably, the polarizability correlated poorly with the aggregation mode, implying that the vdWs interaction is not a crucial factor in controlling the aggregation morphology. Previous studies also suggested vdWs interaction is weak and could act as a dominant contributor to the overall attractions in the absence of  $\pi$ - $\pi$  interaction.<sup>66</sup> For the aggregation of GO,  $\pi$ - $\pi$  stacking would be more important than vdWs, and there is

no significant association between vdWs interaction and the distinct aggregation morphology under different aqueous chemistries.

#### H-bond interaction

Based on previous studies<sup>37, 57</sup>, there are two kinds of H-bond that will mediate the aggregation: direct H-bond formed between functional groups of GO, and water-bridged H-bond formed between water and the functional groups of GO. For example, hydroxy (OH) and deprotonated carboxyl (COO<sup>-</sup>) can form direct OH $\cdots$ COO<sup>-</sup> H-bond and water-bridged OH $\cdots$ water $\cdots$ COO<sup>-</sup> H-bond. OH $\cdots$ COO<sup>-</sup> will change to OH $\cdots$ COOH at lower pH and COO<sup>-</sup> will coordinate with the metal ions added, thus, both the direct and water-bridged H-bond intensity will be affected upon protonation and the presence of metal ions. Fig.5 and SI7 listed all the direct and water-bridged H-bonds properties with and without the interference of protonation and metal ions, and the intensity of H-bond was examined according to the classification of Jerrey<sup>67</sup> that H-bonds with shorter length and larger angle are considered as stronger H-bond interactions. Notably, upon protonation and the binding with metal ions, properties of the direct and water-bridged H-bonds were changed. However, no significant correlation was found between strength of H-bonds and the aggregation mode. For example (Fig.5), protonation showed a more significant effect in impairing the OH $\cdots$ COO<sup>-</sup> direct H-bond and coordination with metal ions showed a more significant effect in accelerating the COO<sup>-</sup> $\cdots$ COO<sup>-</sup> water-bridged H-bond, both of which are contrary to the trend that protonation is more effective in facilitating the stackings of GO. Therefore, it is concluded that GO tend to aggregate in the face-to-face mode at lower pH is not relate to the H-bond interaction.

#### Water-mediated inhibition

Except for the above driving forces, steering force co-existed during the aggregation. More specifically, the oxygen-containing functional groups facilitate water molecules to bind with GO by forming H-bond, and the aggregation could be viewed as a competition between GO and water to the surface of another GO. Water molecules arrive at the GO earlier and form H-bond network with hydrophilic functional groups. Thus, before aggregation, GOs have to break the H-bond network and squeeze out the water clusters. Along these lines, if GO bind with water molecules strongly, the aggregation will be inhibited. Therefore, it was inferred that protonation and binding with metal ions have different effect on the binding strength of GO with water molecules. To verify this hypothesis, MD simulations were performed to calculate the amount of H-bond formed between GO and water, and DFT calculations to examine the intensity of the H-bonds.

As shown in Fig. 6a, upon protonation, amount of H-bond formed between GO and water decreased from  $\sim$ 185 to  $\sim$ 160, implying protonation can effectively decrease the amount of water binding on GO. However, no significant changes occur when Ca<sup>2+</sup> or Na<sup>+</sup> were added. To further explore the strength of the binding between GO and water, length and angle of the H-bonds were calculated. As shown in Fig. 6b, intensities of the hydroxy $\cdots$ water and epoxy $\cdots$ water were significantly decreased upon protonation compared to binding with metal ions. Therefore, protonation is more efficient in decrease the interaction intensity between hydroxy and epoxy with water. It should be noted that the no significant correlation was found between the change of carboxyl $\cdots$ water H-bond intensity and

the amount of GO-water H-bond, therefore, the decreased amount of GO-water H-bond under protonation is mainly due to the impaired intensity of hydroxy...water and epoxy...water H-bond. Considering the binding amount and binding intensity, it is concluded that protonation is more efficient in impairing the binding between GO and water. Therefore, the water-mediated inhibition is also a crucial factor in controlling the aggregation morphology.

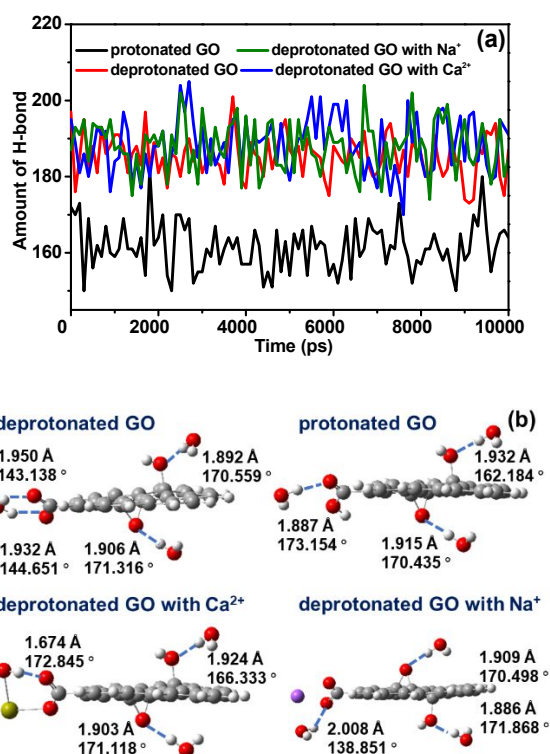


**Fig. 6.** Effect of protonation and metal ions on the amount (a) and intensity (b) of H-bond formed between GO and water. Blue dashed lines in (b) are H-bonds.

Additional to the morphology, aggregation kinetic was also related to the mechanisms. The strengthened  $\pi$ - $\pi$  and vdWs upon protonation correlate well with the accelerated aggregation kinetic at lower pH, indicating  $\pi$ - $\pi$  and vdWs are important in mediating the aggregation kinetic. And the evolution of H-bond demonstrated it failed to play key roles. Water-mediated inhibition is related to the hydrophobicity, that the inhibition is more significant for GO with lower hydrophobicity<sup>40</sup>. Therefore, the suppressed water-mediated inhibition also contributed to the aggregation kinetic at lower pH. Combined previous studies and the results in the current study, it is concluded that the accelerated aggregation kinetic at lower pH was determined by electrostatic repulsion,  $\pi$ - $\pi$ , vdWs, and water-mediated inhibition. The evolution of  $\pi$ - $\pi$  and water-mediated inhibition correlated poorly with the fact that metal ions promoted the aggregation kinetic of GO. And it is concluded that the accelerated aggregation kinetic with the presence of metal ions was mainly related to the electrostatic repulsion, vdWs, and GO-metal interactions.

It has been recognized that many aggregation processes are fractal in nature, including GO<sup>68</sup>. The fractal dimension depends on the

collision efficiency, and the aggregate formation and structure is related to aggregation kinetics. According to the fractal theory, aggregate with more compact structure possess higher fractal dimension<sup>69</sup>. Based on the AFM and MD results, it is inferred aggregates that are formed from protonation and coordination with metal ions would have different fractal dimension values. The protonation induced face-to-face or partial face-to-face aggregation would form more compact aggregate considering less water molecules were confined within the interlayer compared to other aggregation mode. In addition, fractal dimension may change during the aggregation. In our future studies, MD and fractal dimension measurements will be combined to elucidate the relationship between evolution of fractal dimension and the dynamic aggregation process.

## Conclusions

This study combined MD simulations, DFT calculations, and AFM measurement to investigate the favourable aggregation mode of GO under different aqueous chemistries. Four kinds of aggregate mode during the aggregation process were revealed: face-to-face, partial face-to-face, edge-to-edge, and point-to-point. pH and metal ions can exert distinct effects on the aggregation mode of GO, and the main mechanism of the is that lower pH can effectively accelerate the  $\pi$ - $\pi$  interaction and impair the water-mediated steric hindrance.

Revealing the aggregation pattern is valuable for elucidating the aggregation mechanisms of GO and other GO-based materials. Also, a detailed understanding of the favourable aggregation mode under different aqueous environment is critical for predicting the toxicity. For example, concentration of monovalent ions ( $\text{Na}^+$ ,  $\text{K}^+$ ) is less than 10 mM and pH are 5~9 in most natural freshwater bodies, therefore, GO may disperse or aggregate in the edge-to-edge or point-to-point mode. Thus, the shading effect will not be alleviated, and the aggregation will not affect GO toxicity mechanism towards algae. Additionally, if GO is utilized as adsorbent for organic pollutant removal, elucidating the GO aggregation mode helps to link the aggregation and adsorption behaviours. Specifically, if face-to-face aggregation dominates, aggregation of GO may help to capture organic molecules and form GO/organic/GO sandwich-like adsorption configuration. In addition, the combination of MD, DFT, and AFM in this study can provide a new platform for investigating the aggregation behaviour of nanomaterials in water and maybe in other media too.

This work focus on the effect of pH and metal ions on the aggregation morphology of small flakes of GO, other factors, such as GO composition (oxygen content, composition of the functional group), GO structure (wrinkles and imperfections), and natural organic matter may also have effect on the aggregation morphology, and should be considered in our future study. Moreover, further study is needed to provide details for the toxicity and adsorption property of GOs with different aggregation mode.

## Conflicts of interest

There are no conflicts to declare

## Acknowledgements

This paper is supported by the National Natural Science Foundation of China (51908447), China Postdoctoral Science Foundation (2019M663650), The Youth Innovation Team of Shaanxi Universities, Shaanxi Provincial Key Research and Development Project (2018ZDXM-SF-020), and USDA-NIFA Hatch program (MAS 00475).

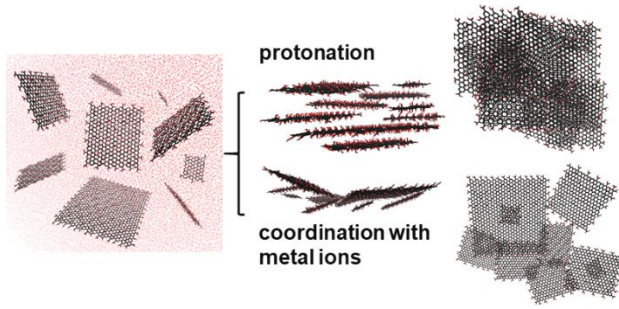
## Notes and references

- D. R. Dreyer, S. Park, C. W. Bielawski and R. S. Ruoff, The chemistry of graphene oxide, *Chemical society reviews*, 2010, **39**, 228-240.
- J. Zhang, Y. Li, X. Xie, W. Zhu and X. Meng, Fate of adsorbed Pb (II) on graphene oxide under variable redox potential controlled by electrochemical method, *Journal of hazardous materials*, 2019, **367**, 152-159.
- S. J. Rowleyneale, E. P. Randviir, A. S. A. Dena and C. E. Banks, An overview of recent applications of reduced graphene oxide as a basis of electroanalytical sensing platforms, *Applied Materials Today*, 2017, **10**, 218-226.
- V. Georgakilas, J. N. Tiwari, K. C. Kemp, J. A. Perman, A. B. Bourlinos, K. S. Kim and R. Zboril, Noncovalent functionalization of graphene and graphene oxide for energy materials, biosensing, catalytic, and biomedical applications, *Chemical reviews*, 2016, **116**, 5464-5519.
- V. Chabot, D. Higgins, A. Yu, X. Xiao, Z. Chen and J. Zhang, A review of graphene and graphene oxide sponge: material synthesis and applications to energy and the environment, *Energy & Environmental Science*, 2014, **7**, 1564-1596.
- A. Ghaffar, L. Zhang, X. Zhu and B. Chen, Scalable graphene oxide membranes with tunable water channels and stability for ion rejection, *Environmental science. Nano*, 2019, **6**, 904-915.
- M. Checa, M. Figueredo, A. Aguinaco and F. J. Beltran, Graphene oxide/titania photocatalytic ozonation of primidone in a visible LED photoreactor, *Journal of Hazardous Materials*, 2019, **369**, 70-78.
- Z. Cai, A. D. Dwivedi, W.-N. Lee, X. Zhao, W. Liu, M. Sillanpää, D. Zhao, C.-H. Huang and J. Fu, Application of nanotechnologies for removing pharmaceutically active compounds from water: development and future trends, *Environmental Science: Nano*, 2018, **5**, 27-47.
- Graphene Market Size, <https://www.grandviewresearch.com/industry-analysis/graphene-industry>.
- A. S. Adeleye, K. T. Ho, M. Zhang, Y. Li and R. M. Burgess, Fate and Transformation of Graphene Oxide in Estuarine and Marine Waters, *Environmental Science & Technology*, 2019, **53**, 5858-5867.
- G. D. Jr, A. S. Adeleye, L. Sung, K. T. Ho, R. M. Burgess and E. J. Petersen, Detection and Quantification of Graphene-Family Nanomaterials in the Environment, *Environmental Science & Technology*, 2018, **52**, 4491-4513.
- P. F. M. Nogueira, D. Nakabayashi and V. Zucolotto, The effects of graphene oxide on green algae *Raphidocelis subcapitata*, *Aquatic Toxicology*, 2015, **166**, 29-35.
- C. Hu, Q. Wang, H. Zhao, L. Wang, S. Guo and X. Li, Ecotoxicological effects of graphene oxide on the protozoan *Euglena gracilis*, *Chemosphere*, 2015, **128**, 184-190.
- J. Zhao, X. Cao, Z. Wang, Y. Dai and B. Xing, Mechanistic understanding toward the toxicity of graphene-family materials to freshwater algae, *Water Research*, 2017, **111**, 18-27.
- Y. Ai, Y. Liu, Y. Huo, C. Zhao, L. Sun, B. Han, X. Cao and X. Wang, Insights into the adsorption mechanism and dynamic behavior of tetracycline antibiotics on reduced graphene oxide (RGO) and graphene oxide (GO) materials, *Environmental science. Nano*, 2019.
- N. Yousefi, X. Lu, M. Elimelech and N. Tufenkji, Environmental performance of graphene-based 3D macrostructures, *Nature Nanotechnology*, 2019, **14**, 107-119.
- A. Ghaffar, L. Zhang, X. Zhu and B. Chen, Scalable graphene oxide membranes with tunable water channels and stability for ion rejection, *Environmental Science: Nano*, 2019, **6**, 904-915.
- X. Zhu, K. Yang and B. Chen, Membranes prepared from graphene-based nanomaterials for sustainable applications: a review, *Environmental Science: Nano*, 2017, **4**, 2267-2285.
- H. Zhang, Y. Zhu, J. Long, Z. Ding, R. Yuan, Z. Li and C. Xu, In situ construction of layered graphene-based nanofiltration membranes with interlayer photocatalytic purification function and their application for water treatment, *Environmental Science: Nano*, 2019, **6**, 2195-2202.
- R. L. D. Whitby, Chemical Control of Graphene Architecture: Tailoring Shape and Properties, *ACS Nano*, 2014, **8**, 9733-9754.
- Y. Qi, W. Chen, F. Liu, J. Liu, T. Zhang and W. Chen, Aggregation morphology is a key factor determining protein adsorption on graphene oxide and reduced graphene oxide nanomaterials, *Environmental science. Nano*, 2019, **6**, 1303-1309.
- Y. Jiang, R. Raliya, P. Liao, P. Biswas and J. D. Fortner, Graphene oxides in water: assessing stability as a function of material and natural organic matter properties, *Environmental science. Nano*, 2017, **4**, 1484-1493.
- X. Ren, J. Li, C. Chen, Y. Gao, D. Chen, M. Su, A. Alsaedi and T. Hayat, Graphene analogues in aquatic environments and porous media: dispersion, aggregation, deposition and transformation, *Environmental science. Nano*, 2018, **5**, 1298-1340.
- K. Yang, B. Chen, X. Zhu and B. Xing, Aggregation, adsorption, and morphological transformation of graphene oxide in aqueous solutions containing different metal cations, *Environmental science & technology*, 2016, **50**, 11066-11075.
- Y. Jiang, R. Raliya, J. D. Fortner and P. Biswas, Graphene Oxides in Water: Correlating Morphology and Surface Chemistry with Aggregation Behavior, *Environmental Science & Technology*, 2016, **50**, 6964-6973.
- I. Chowdhury, M. C. Duch, N. D. Mansukhani, M. C. Hersam and D. Bouchard, Colloidal properties and stability of graphene oxide nanomaterials in the aquatic environment, *Environmental Science & Technology*, 2013, **47**, 6288-6296.
- L. J. Cote, F. Kim and J. Huang, Langmuir-Blodgett Assembly of Graphite Oxide Single Layers, *Journal of the American Chemical Society*, 2009, **131**, 1043-1049.
- S. Liu, T. H. Zeng, M. Hofmann, E. Burcombe, J. Wei, R. Jiang, J. Kong and Y. Chen, Antibacterial activity of graphite, graphite oxide, graphene oxide, and reduced graphene oxide: membrane and oxidative stress, *ACS nano*, 2011, **5**, 6971-6980.
- S. Das, S. Singh, V. Singh, D. Joung, J. M. Dowding, D.

- Reid, J. Anderson, L. Zhai, S. I. Khondaker and W. T. Self, Oxygenated functional group density on graphene oxide: its effect on cell toxicity, *Particle & Particle Systems Characterization*, 2013, **30**, 148-157.
30. Z. Jian, W. Zhenyu, J. C. White and X. Baoshan, Graphene in the aquatic environment: adsorption, dispersion, toxicity and transformation, *Environmental Science & Technology*, 2014, **48**, 9995-10009.
31. G. Sigmund, C. Jiang, T. Hofmann and W. Chen, Environmental transformation of natural and engineered carbon nanoparticles and implications for the fate of organic contaminants, *Environmental science. Nano*, 2018, **5**, 2500-2518.
32. H. Tang, Y. Zhao, S. Shan, X. Yang, D. Liu, F. Cui and B. Xing, Wrinkle- and Edge-Adsorption of Aromatic Compounds on Graphene Oxide as Revealed by Atomic Force Microscopy, Molecular Dynamics Simulation, and Density Functional Theory, *Environmental Science & Technology*, 2018, **52**, 7689-7697.
33. T. Lan, J. Liao, Y. Yang, Z. Chai, N. Liu and D. Wang, Competition/Cooperation between Humic Acid and Graphene Oxide in Uranyl Adsorption Implicated by Molecular Dynamics Simulations, *Environmental Science & Technology*, 2019, **53**, 5102-5110.
34. Y. Tu, M. Lv, P. Xiu, T. Huynh, M. Zhang, M. Castelli, Z. Liu, Q. Huang, C. Fan and H. Fang, Destructive extraction of phospholipids from *Escherichia coli* membranes by graphene nanosheets, *Nature nanotechnology*, 2013, **8**, 594.
35. G. Fang, B. Luan, C. Ge, Y. Chong, X. Dong, J. Guo, C. Tang and R. Zhou, Understanding the graphene quantum dots-ubiquitin interaction by identifying the interaction sites, *Carbon*, 2017, **121**, 285-291.
36. S. Yu, X. Wang, W. Yao, J. Wang, Y. Ji, Y. Ai, A. Alsaedi, T. Hayat and X. Wang, Macroscopic, spectroscopic, and theoretical investigation for the interaction of phenol and naphthol on reduced graphene oxide, *Environmental Science & Technology*, 2017, **51**, 3278-3286.
37. H. Tang, Y. Zhao, S. Shan, X. Yang, D. Liu, F. Cui and B. Xing, Theoretical insight into the adsorption of aromatic compounds on graphene oxide, *Environmental science. Nano*, 2018, **5**, 2357-2367.
38. Q. Zhou, S. Ouyang, Z. Ao, J. Sun, G. Liu and X. Hu, Integrating Biolayer Interferometry, Atomic Force Microscopy, and Density Functional Theory Calculation Studies on the Affinity between Humic Acid Fractions and Graphene Oxide, *Environmental Science & Technology*, 2019, **53**, 3773-3781.
39. N. I. Kovtyukhova, P. J. Ollivier, B. R. Martin, T. E. Mallouk, S. A. Chizhik, E. V. Buzaneva and A. D. Gorchinskiy, Layer-by-layer assembly of ultrathin composite films from micron-sized graphite oxide sheets and polycations, *Chem Mater*, 1999, **11**, 771-778.
40. H. Tang, Y. Zhao, X. Yang, D. Liu, P. Shao, Z. Zhu, S. Shan, F. Cui and B. Xing, New Insight into the Aggregation of Graphene Oxide Using Molecular Dynamics Simulations and Extended Derjaguin-Landau-Verwey-Overbeek Theory, *Environmental Science & Technology*, 2017, **51**, 9674-9682.
41. J. M. Montgomery, *Water treatment: principles and design*, John Wiley & Sons, 1985.
42. A. Lerf, H. He, M. Forster and J. Klinowski, Structure of graphite oxide revisited, *The Journal of Physical Chemistry B*, 1998, **102**, 4477-4482.
43. L. Wang, K. Lee, Y.-Y. Sun, M. Lucking, Z. Chen, J. J. Zhao and S. B. Zhang, Graphene oxide as an ideal substrate for hydrogen storage, *ACS nano*, 2009, **3**, 2995-3000.
44. N. Wei, C. Lv and Z. Xu, Wetting of graphene oxide: A molecular dynamics study, *Langmuir*, 2014, **30**, 3572-3578.
45. H. Tang, Y. Zhao, X. Yang, D. Liu, S. Shan and F. Cui, Understanding the roles of solution chemistries and functionalization on the aggregation of graphene-based nanomaterials using molecular dynamic simulations, *The Journal of Physical Chemistry C*, 2017, **121**, 13888-13897.
46. W. L. Jorgensen, D. S. Maxwell and J. Tirado-Rives, Development and testing of the OPLS all-atom force field on conformational energetics and properties of organic liquids, *J Am Chem Soc*, 1996, **118**, 11225-11236.
47. D. Van Der Spoel, E. Lindahl, B. Hess, G. Groenhof, A. E. Mark and H. J. Berendsen, GROMACS: fast, flexible, and free, *J Comput Chem*, 2005, **26**, 1701-1718.
48. H. Berendsen, J. Grigera and T. Straatsma, The missing term in effective pair potentials, *Journal of Physical Chemistry*, 1987, **91**, 6269-6271.
49. B. Hess, H. Bekker, H. J. Berendsen and J. G. Fraaije, LINCS: a linear constraint solver for molecular simulations, *J Comput Chem*, 1997, **18**, 1463-1472.
50. M. S. K. P. SETTLE, An analytical version of the SHAKE and RATTLE algorithm for rigid water molecules, *J. Comput. Chem*, 1992, **13**, 952-962.
51. T. Darden, D. York and L. Pedersen, Particle mesh Ewald: An  $N \cdot \log(N)$  method for Ewald sums in large systems, *The Journal of chemical physics*, 1993, **98**, 10089-10092.
52. M. Parrinello and A. Rahman, Polymorphic transitions in single crystals: A new molecular dynamics method, *Journal of Applied physics*, 1981, **52**, 7182-7190.
53. W. Lysenko, *Equilibrium phase-space distributions*, 1978.
54. H. J. Berendsen, J. v. Postma, W. F. van Gunsteren, A. DiNola and J. Haak, Molecular dynamics with coupling to an external bath, *The Journal of chemical physics*, 1984, **81**, 3684-3690.
55. A. Luzar and D. Chandler, Hydrogen-bond kinetics in liquid water, *Nature*, 1996, **379**, 55-57.
56. M. Chen, X. Lu, X. Liu, Q. Hou, Y. Zhu and H. Zhou, Retardation of Water Reorientation at the Oil/Water Interface, *J Phys Chem C*, 2015, **119**, 16639-16648.
57. H. Tang, D. Liu, Y. Zhao, X. Yang, J. Lu and F. Cui, Molecular dynamics study of the aggregation process of graphene oxide in water, *The Journal of Physical Chemistry C*, 2015, **119**, 26712-26718.
58. H. Tang, Y. Zhao, X. Yang, D. Liu, S. Shan and F. Cui, Understanding the Roles of Solution Chemistries and Functionalization on the Aggregation of Graphene-Based Nanomaterials Using Molecular Dynamic Simulations, *J Phys Chem C*, 2017.
59. M. Frisch, G. Trucks, H. Schlegel, G. Scuseria, M. Robb, J. Cheeseman, G. Scalmani, V. Barone, B. Mennucci and G. Petersson, Gaussian 09, revision D. 01. *Journal*, 2009.
60. T. Lu and F. Chen, Multiwfn: a multifunctional wavefunction analyzer, *J Comput Chem*, 2012, **33**, 580-592.
61. L. Wu, L. Liu, B. Gao, R. Muñoz-Carpena, M. Zhang, H. Chen, Z. Zhou and H. Wang, Aggregation kinetics of graphene oxides in aqueous solutions: experiments, mechanisms, and modeling, *Langmuir*, 2013, **29**, 15174-15181.
62. H. Tang, Y. Zhao, X. Yang, D. Liu, P. Shao, Z. Zhu, S. Shan, F. Cui and B. Xing, New Insight into the Aggregation of Graphene Oxide Using Molecular

- 1  
2  
3 Dynamics Simulations and Extended Derjaguin–Landau–  
4 Verwey–Overbeek Theory, *Environmental Science &*  
5 *Technology*, 2017, **51**, 9674-9682.
- 6 63. L. M. Salonen, M. Ellermann and F. Diederich, Aromatic  
7 rings in chemical and biological recognition: energetics  
8 and structures, *Angewandte Chemie International Edition*,  
9 2011, **50**, 4808-4842.
- 10 64. J. F. Gonthier, S. N. Steinmann, L. Roch, A. Ruggi, N.  
11 Luisier, K. Severin and C. Corminboeuf,  $\pi$ -Depletion as a  
12 criterion to predict  $\pi$ -stacking ability, *Chem Commun*,  
13 2012, **48**, 9239-9241.
- 14 65. P. Thiyam, C. Persson, B. E. Sernelius, D. F. Parsons, A.  
15 Malthe-Sørensen and M. Boström, Intermolecular  
16 Casimir-Polder forces in water and near surfaces, *Physical*  
17 *Review E*, 2014, **90**, 032122.
- 18 66. G. Ersan, O. G. Apul, F. Perreault and T. Karanfil,  
19 Adsorption of organic contaminants by graphene  
20 nanosheets: A review, *Water Res*, 2017.
- 21 67. G. A. Jeffrey and G. A. Jeffrey, *An introduction to*  
22 *hydrogen bonding*, Oxford university press New York,  
23 1997.
- 24 68. Z. Hua, Z. Tang, X. Bai, J. Zhang, L. Yu and H. Cheng,  
25 Aggregation and resuspension of graphene oxide in  
26 simulated natural surface aquatic environments,  
27 *Environmental pollution*, 2015, **205**, 161-169.
- 28 69. J. C. Crittenden, R. R. Trussell, D. W. Hand, K. J. Howe  
29 and G. Tchobanoglous, *MWH's water treatment:*  
30 *principles and design*, John Wiley & Sons, 2012.
- 31  
32  
33  
34  
35  
36  
37  
38  
39  
40  
41  
42  
43  
44  
45  
46  
47  
48  
49  
50  
51  
52  
53  
54  
55  
56  
57  
58  
59  
60

Aggregation mode mediated by protonation and metal cations



1  
2  
3  
4  
5  
6  
7  
8  
9  
10  
11  
12  
13  
14  
15  
16  
17  
18  
19  
20  
21  
22  
23  
24  
25  
26  
27  
28  
29  
30  
31  
32  
33  
34  
35  
36  
37  
38  
39  
40  
41  
42  
43  
44  
45  
46  
47  
48  
49  
50  
51  
52  
53  
54  
55  
56  
57  
58  
59  
60